

Characteristics of the curvature effect of uniform jets or spherical fireballs

R.-J. Lu^{1,2,3,4}, Y.-P. Qin^{1,2,4}

¹*National Astronomical Observatories/Yunnan Observatory, Chinese Academy of Sciences,
P. O. Box 110, Kunming 650011, China*

²*Physics Department, Guangxi University, Nanning, Guangxi 530004, P.R. China*

³*The Graduate School of the Chinese Academy of Sciences; luruijing@126.com*

⁴*E-mail: luruijing@126.com, ypqin@public.km.yn.cn*

Accepted 0000. Received 0000; in original form 2005 August 08

ABSTRACT

Qin et al. (2004) have derived a formula of count rates based on a model of highly symmetric expanding fireballs, where the Doppler effect is the key factor to be concerned. In this paper, we employ the formula to both the Qin model and the uniform jet model to study how the rising timescale, $\Delta\tau_{\theta,r}$, and the decay timescale, $\Delta\tau_{\theta,d}$, of a local pulse affect the light curve of GRBs. Our analysis shows that they do make contributions to both rising and decay portions of the light curve of GRBs. Associated with a local pulse with both rising and decay portions, the light curve of GRBs in the rising portion is expected to undergo a concave phase and then a convex one, which we call a “concave-to-convex” character, whereas that in the decay portion is expected to evolve an opposite process which is called a “convex-to-concave” character, regardless of being in Qin model or in the uniform jet model. These characteristics are independent of local pulse shapes and their rest frame radiation forms. The diversity of light curves are caused by different forms of local pulses and different ratios of $\Delta\tau_{\theta,r}$ to $\Delta\tau_{\theta,d}$. We study a sample of 86 GRB pulses detected by the BATSE instrument on board the Compton Gamma Ray Observatory and find that the “concave-to-convex” (expected in the rising portion of the light curve) and “convex-to-concave” (expected in the decay portion) characters, which result from the curvature effect of spherical surface (or the Doppler effect), do exist in the light curve of some GRBs.

Key words: GRBs gamma-ray: bursts —methods: data analysis

1 INTRODUCTION

Light curves of gamma-ray bursts (GRBs) vary drastically in morphology. Only less than 10 percent of the light curve profiles detected by the BATSE instrument on board the Compton Gamma Ray Observatory (CGRO) can be categorized as being similar in the overall shape. A pulse in the gamma-ray light curve is generally considered to result from an individual shock episode. Superposition of many such pulses is believed to create the observed diversity and complexity of light curves, which could not be describable by a simple formula. Therefore, the temporal characteristics of these pulses hold the key to the understanding of the prompt radiation of GRBs.

Some well-separated pulses are seen to comprise a fast rise and an exponential decay (FRED) (Fishman et al. 1994). Many attempts have been made to decompose the complex light curves into pulses, which can be described by several flexible functions based on empirical or semi-empirical relations, and quantify their characteristics (e.g., Norris et al. 1996; Femimore et al. 1996; Lee et al. 2000a, 2000b; Ryde & Svensson 2000, 2002; Ryde & Petrosian 2002; Borgonovo & Ryde 2001; Kocevski et al. 2003, hereafter Paper I). E.g., as derived in detail in Paper I, a FRED pulse could be well described by equation (22) or (28), and using this model, they revealed some features of the profiles of individual GRB pulses.

However what physics causes such a observed profiles? According to Ryde & Petrosian (2002), the simplest scenario accounting for the observed GRB pulses is to assume an impulsive heating of the leptons and a subsequent cooling and emission. In this scenario, the rising phase of the pulse, which is referred to as the dynamic time, arises from the energizing of the shell, while the decay phase reflects the cooling and its timescale. However, in general, the cooling time for the relevant parameters is too short to explain the pulse durations and the resulting cooling spectra are not consistent with observation (Ghisellini et al. 2000). As shown by Ryde & Petrosian (2002), this problem could be solved when the curvature effect of the expanding fireball surface is taken into account.

However, there is no consensus on what effects lie behind the observed pulse shapes. We suspect that the pulse shapes might have some relations to their counterparts. Motivated by this, we explore in this paper possible explanations for the pulse shapes observed based on the curvature effect (or the Doppler effect of fireballs).

Due to the observed output rate of radiation, the observed gamma-ray pulses are believed to be produced in a highly relativistic outflow, (e.g., an expanding and collimated fireball),

based on the large energies and the short timescales involved. In the case of a spherical fireball, the Doppler effect over the whole fireball must be at work, and the observed FRED structure probably provide the intrinsical information. Qin (2002) has derived the flux function based on the model of highly symmetric expanding fireball, where the Doppler effect of the expanding fireball surface is the key factor to be concerned, and then with this formula, Qin (2003) studied how emission and absorbtion lines are affect by the effect. Recently, Qin et al. (2004) presented the formula in terms of count rates. Based on their model, many characteristics of profiles of observed gamma-ray burst pulses could be explained. They convince us that the exponential decay phase of the FRED pulse arises from the time delay of different parts of the surface and its rising portion is produced by the width of a local pulse. However, some interesting questions, such as what a role the rising and decay portions of local pulses play in the observed light curve of gamma-ray bursts, and what are responsible for the diversity of the FRED pulses, urge us to investigate in a much detail.

Jets in GRBs were first suggested by Waxman et al. (1998), and then they were widely evoked to explain its spectacular energy release (e.g.,Fruchter et al. 1999). Subsequent multiwavelength observations of GRBs have been interpreted as evidence for explosions with jet-like geometry (Stanek et al. 1999; Harrison et al. 1999). Recently, two phenomenological models of GRB jets received widespread attention: a uniform jet model in which the emissivity is a constant independent of the angle relative to the jet axis (Frail et al. 2001;Panaitescu & Kumar 2001; Rossi et al. 2002; Zhang et al. 2002; Bloom et al. 2003; Zhang et al. 2004a, 2004b), and a structure jet model in which the emissivity is a function of the angle relative to the jet axis (Frail et al. 2001; Rmairez-Ruiz et al. 2002; Lamb et al. 2005). In the case of a uniform jet, the formula presented in Qin et al. (2004) could be applicable as long as the open angle of the jet is taken into account.

According to the relativistic fireball model, the emission from a spherically expanding shell and a jet would be rather similar to each other as long as we are along the jet's axis and the Lorentz factor Γ of the relativistic motion satisfies $\Gamma^{-1} < \theta_j$, because the matter does not have enough time (in its own rest frame) to expand sideways at such situation (Piran 1995).

The detection of very energetic photons (in the GeV range) in several gamma-ray bursts (GRBs) and the very short variability timescale (Fishman et al. 1995), sometimes less than 1 ms, exhibited by the 100 keV emission of many bursts have led to the conclusion that they arise from sources that are moving at extremely relativistic speeds, with very large Lorentz

factors Γ that could exceed 100 (Fenimore, Epstein, & Ho 1993; Piran 1999). At the same time, From the derived parameter, θ_j , of the sample of 41 source in Friedman et al. (2004), we find that the range of θ_j is $\{0.03107, 0.57072\}$ rad, and its average value is 0.15925 rad. The data show that $\Gamma^{-1} < \theta_j$ if $\Gamma > 100$. In this paper, we assume that the condition of $\Gamma^{-1} < \theta_j$ is satisfied for all the source concerned.

This paper is organized as follows. In section 2, we present the characteristics of the light curve of GRBs obtained from our theoretical analysis based on a uniform jet and a spherical fireball model. In section 3, we examine the characteristics of light curves of a group of source detected by the BATSE instrument on board the Compton Gamma Ray Observatory. Discussion and conclusions will be presented in the last section.

2 NUMERICAL ANALYSIS

As derived in detail in Qin et al. (2004), the expected count rate of the fireball within frequency interval $[\nu_1, \nu_2]$ can be calculated with equation (21), which is as follows:

$$C(\tau) = \frac{2\pi R_c^3 \int_{\tilde{\tau}_{\theta, \min}}^{\tilde{\tau}_{\theta, \max}} \tilde{I}(\tau_{\theta})(1 + \beta\tau_{\theta})^2(1 - \tau + \tau_{\theta})d\tau_{\theta} \int_{\nu_1}^{\nu_2} \frac{g_{0,\nu}(\nu_{0,\theta})}{\nu} d\nu}{hcD^2\Gamma^3(1 - \beta)^2(1 + k\tau)^2}, \quad (1)$$

where $\tilde{I}(\tau_{\theta})$ represents the development of the intensity magnitude in the observer frame, called as a local pulse function, $g_{0,\nu}(\nu_{0,\theta})$ describes the rest frame radiation mechanisms, and τ is confined by $1 - \cos\theta_{\min} + (1 - \beta \cos\theta_{\min})\tau_{\theta, \min} \leq \tau \leq 1 - \cos\theta_{\max} + (1 - \beta \cos\theta_{\max})\tau_{\theta, \max}$, while $\tilde{\tau}_{\theta, \min}$ and $\tilde{\tau}_{\theta, \max}$ are determined by $\tilde{\tau}_{\theta, \min} = \max\{\tau_{\theta, \min}, \frac{\tau - 1 + \cos\theta_{\max}}{1 - \beta \cos\theta_{\max}}\}$ and $\tilde{\tau}_{\theta, \max} = \min\{\tau_{\theta, \max}, \frac{\tau - 1 + \cos\theta_{\min}}{1 - \beta \cos\theta_{\min}}\}$, respectively. we will employ equation (1) in the following analysis.

2.1 In the case of radiation emitted from the whole fireball surface

If the radiation is emitted from the whole fireball surface, we can take $\theta_{\min} = 0$ and $\theta_{\max} = \pi/2$. Therefore the range of τ is $(1 - \beta)\tau_{\theta, \min} \leq \tau \leq 1 + \tau_{\theta, \max}$, while $\tilde{\tau}_{\theta, \min}$ and $\tilde{\tau}_{\theta, \max}$ are determined by $\tilde{\tau}_{\theta, \min} = \max\{\tau_{\theta, \min}, \tau - 1\}$ and $\tilde{\tau}_{\theta, \max} = \min\{\tau_{\theta, \max}, \tau/(1 - \beta)\}$, respectively.

Formula (1) suggests that, except the state of the fireball (i.e., Γ , R_c and D), light curves of sources depend on $\tilde{I}(\tau_{\theta})$ and $g_{0,\nu}(\nu_{0,\theta})$. We assume in this paper the common empirical radiation form of GRBs as the rest frame radiation form, the so-called Band function (Band et al. 1993) that was frequently, and rather successfully employed to fit the spectra of sources (see, e.g., Schaefer et al. 1994; Ford et al. 1995; Preece et al. 1998, 2000). We focus our attention to the roles that the rising and decay portions of local pulses play in the light

curve of gamma-ray bursts. Several forms of local pulses would be employed to study this issue.

(a) Local pulse with a power law rise and a power law decay

A power law form of $\tilde{I}(\tau_\theta)$ is adopted as follows:

$$\tilde{I}(\tau_\theta) = I_0 \begin{cases} \left(\frac{\tau_\theta - \tau_{\theta,\min}}{\tau_{\theta,0} - \tau_{\theta,\min}}\right)^\mu & (\tau_{\theta,\min} \leq \tau_\theta \leq \tau_{\theta,0}) \\ \left(1 - \frac{\tau_\theta - \tau_{\theta,0}}{\tau_{\theta,\max} - \tau_{\theta,0}}\right)^\mu & (\tau_{\theta,0} < \tau_\theta \leq \tau_{\theta,\max}) \end{cases} \quad (2)$$

For this local pulse we find that $\Delta\tau_{\theta,FWHM} = (1 - 2^{-1/\mu})(\tau_{\theta,\max} - \tau_{\theta,\min})$ and therefore, $\tau_{\theta,\max} = \frac{\Delta\tau_{\theta,FWHM}}{(1 - 2^{-1/\mu})} + \tau_{\theta,\min}$.

For a given value of $\tau_{\theta,\max}$, the rising timescale, $\Delta\tau_{\theta,r}$, and the decay timescale $\Delta\tau_{\theta,d}$ of a local pulse vary with the shift of the position of $\tau_{\theta,0}$, where $\Delta\tau_{\theta,r}$ and $\Delta\tau_{\theta,d}$ are the FWHM widths in the rising and decay portions, respectively. We assign

$$\tau_{\theta,0} = \tau_{\theta,\min} + e(\tau_{\theta,\max} - \tau_{\theta,\min}), \text{ where } 0 \leq e \leq 1. \quad (3)$$

We find that $\Delta\tau_{\theta,r} = \tau_{\theta,0} - \tau_{\theta,\min}$, $\Delta\tau_{\theta,d} = \tau_{\theta,\max} - \tau_{\theta,0}$. Let

$$r_{rd}(e) = \frac{\Delta\tau_{\theta,r}}{\Delta\tau_{\theta,d}} \quad (4)$$

Quantity $r_{rd}(e)$ denotes the ratio of the rise timescale to the decay timescale of a local pulse.

To describe different contributions of $\Delta\tau_{\theta,r}$ and $\Delta\tau_{\theta,d}$ of a local pulse to the light curve, we define

$$C_r(\tau) = \frac{2\pi R_c^3 \int_{\tau_{\theta,\min}}^{\tau_{\theta,\max}} \tilde{I}(\tau_\theta) (1 + \beta\tau_\theta)^2 (1 - \tau + \tau_\theta) d\tau_\theta \int_{\nu_1}^{\nu_2} \frac{g_{0,\nu}(\nu_{0,\theta})}{\nu} d\nu}{hcD^2\Gamma^3(1 - \beta)^2(1 + k\tau)^2}, \text{ when } (\tau_\theta \leq \tau_{\theta,0}) \quad (5)$$

$$C_d(\tau) = \frac{2\pi R_c^3 \int_{\tau_{\theta,\min}}^{\tau_{\theta,\max}} \tilde{I}(\tau_\theta) (1 + \beta\tau_\theta)^2 (1 - \tau + \tau_\theta) d\tau_\theta \int_{\nu_1}^{\nu_2} \frac{g_{0,\nu}(\nu_{0,\theta})}{\nu} d\nu}{hcD^2\Gamma^3(1 - \beta)^2(1 + k\tau)^2}, \text{ when } (\tau_\theta > \tau_{\theta,0}) \quad (6)$$

$$r_r = \frac{C_r(\tau)}{C(\tau)} \quad (7)$$

$$r_d = \frac{C_d(\tau)}{C(\tau)} \quad (8)$$

where $C(\tau) = C_r(\tau) + C_d(\tau)$. Quantities $C_r(\tau)$ and $C_d(\tau)$ denote the contributions of the rising timescale and decay timescale of a local pulse to the light curve, respectively.

Notes that when $\mu = 1$, the local pulse (2) would become a linear rising and a linear decay one.

Let us employ the Band function radiation form with $\alpha_0 = -1$ and $\beta_0 = -2.25$, to make the light curve, within the frequency range of $100 \leq \nu/\nu_{0,p} \leq 300$. In order to obtain a more detailed information of a light curve profile, we evaluate the first order derivatives, $C'_r(\tau)$,

$C'_d(\tau)$, $C'(\tau)$, and the second order derivatives $C''_r(\tau)$, $C''_d(\tau)$, $C''(\tau)$, of the count rate $C_r(\tau)$, $C_d(\tau)$, $C(\tau)$, respectively. Their profiles are presented in Fig.1.

As shown in Fig. 1, two phases, A-B and D-E, undergo a concave process as $C''_{AB}(\tau) > 0$ and $C''_{DE}(\tau) > 0$, whereas other two phases, B-C and C-D, evolve a convex one because of $C''_{BC}(\tau) < 0$ and $C''_{CD}(\tau) < 0$. We define

$$r_{cv} = \frac{\tau_{AB}}{\tau_{BC}} \quad (9)$$

to denote the ratio of the two time intervals from concavity to convexity in the rising portion of a light curve, where subscripts “c” and “v” represent concavity and convexity respectively.

We notice that r_{cv} increases linearly with r_{rd} . For example, $r_{cv} \simeq 0.28$ when $r_{rd}=0.2$, $r_{cv} \simeq 0.76$ when $r_{rd}=0.5$, and $r_{cv} \simeq 1.64$ when $r_{rd}=1$. Similarly, r_r increases, from $r_r < r_d$ to $r_r > r_d$, with r_{rd} . We notice that there is an interesting point, B, which is an inflexion from concavity to convexity in the rising phase of the light curve, corresponding to the peak point in the local pulse. Then the rising timescale $\Delta\tau_{\theta,r}$ of a local pulse could be obtained by the location of point B from the corresponding light curve.

We find that both the rising timescale and decay portions of the local pulse make a contribution to both portions of the light curve. The rising portion of the local pulse produces concave phases on both sides of the light curve and creates a spiky profile, whereas the decay one yields a convex phase in the rising portion, and a convex-to-concave phase in the decay portion of the light curve, and gives birth to a smooth profile. In a word, the combinational contributions of both portions of the local pulse lead to a light curve with its rising portion evolving from a concave phase to a convex one (the so-called “concave-to-convex” character), and with its decay portion undergoing an opposite process (the so-called “convex-to-concave” one).

(b) Local pulse with a Gaussian form

Here, we replace $\tilde{I}(\tau_\theta)$ in equation (1) with a Gaussian form, which is as follows:

$$\tilde{I}(\tau_\theta) = I_0 \exp\left[-\left(\frac{\tau_\theta - \tau_{\theta,0}}{\sigma}\right)^2\right] \quad (\tau_{\theta,\min} \leq \tau_\theta). \quad (10)$$

The profiles of the light curve are presented in Fig. 2.

We find that a local pulse with a Gaussian form also produces such a profile of light curves: a “concave-to-convex” shape in the rising portion and a reverse one in the decay portion. The differences are that a Gaussian form makes a smaller curvature than a power law one does in the rising portion of light curves either for the concavity or convexity phases,

and that the value of r_{cv} keeps to be 1.24 because r_{rd} keeps to be 1 for a Gaussian form. However the values of r_r and r_d change with σ .

(c) Local pulse with a δ function

Let us consider the case of $\tilde{I}(\tau_\theta)$ being a local δ function, which is as follows:

$$\tilde{I}(\tau_\theta) = \frac{cI_0}{R_c} \delta(\tau_\theta - \tau_{\theta,0}) \quad (\tau_{\theta,\min} \leq \tau_\theta \leq \tau_{\theta,\max}) \quad (11)$$

Associated with a local δ function pulse, the profile of the light curve can be found in Fig. 1 of Qin et al. (2004). There is no rising portion in the light curve for neither rising nor decay timescale in the δ local pulse. But there is a decay portion due to the curvature effect of the expanding fireball.

Besides the three local pulses discussed above, we also study other forms of local pulses, such as $\mu=2, 3$ in equation (2), as well as an exponential form of local pulses, and so on. The same conclusions hold for all these case (see Fig. 1 and 2). The value of r_{cv} increases linearly with r_{rd} at least in the case of these local forms we investigate. The curvature of the rising portion also changes with different forms of local pulses and different r_{rd} , which are responsible for the diversity of light curves.

2.2 In the case of radiation emitted from a uniform jet

If the radiation is emitted from a jet-like geometry with a half-opening angle θ_j and a spherical surface (a uniform jet), we assume for such a relativistic outflow both the Lorentz factor Γ and the energy per unit solid angle from the jet axis are constant during the GRB phase, and assume that the observer direction is the jet axis. At these assumptions, we are able to apply equation (1) to the uniform jet taking $\theta_{min} = 0$ and $\theta_{max} = \theta$, where θ represents the half-opening angle of the jet.

With $\Gamma=10$ and 100 , $\theta_{min} = 0$ and $\theta_{max} = 1/\Gamma$, we repeat the same work as does in the § 2.1, and find the same characteristics of a light curve of GRBs: a “concave-to-convex” phase in the rising portion and a reverse phase in the decay portion, except that there exist a cutoff tail feature in the decay portion (see Fig.1 in Qin et al. 2004). (the cutoff tail feature does not appear in a light curve when θ_{max} is large enough). The characteristics appear to be the result of the curvature effect regardless of a spherical fireball or a uniform jet as long as its surface, from which the radiation is emitted, is a spherical one.

3 OBSERVATIONAL DATA

To test our analysis mentioned above, we examine the profiles of light curves of GRBs detected by the BATSE instrument on board the CGRO (Compton Gamma Ray Observatory). It is already known that pulses of a GRB show a tendency to self-similarity for different energy band (see, e.g. Norris et al. 1996). Therefore, we study in this paper only the count rate of channel 3.

For each source, the background is estimated by a fit with a polynomial expression using 1.024s resolution data that are available from 10 minutes before the trigger to several minutes after the burst. The data along with the background fit coefficients can be obtained from the CGRO Science Support Center (CGROSSC) at NASA Goddard Space Flight Center through its public archives. After subtracting the background counts, we smooth the data with the DB3 wavelet with the MATLAB software in the level of the third-class decomposition. We select a sample comprising of 86 well-separated pulses from these data, on which almost no other small pulses overlap.

For the sake of comparison, the selected pulses above are normalized and their variables, t , are re-scaled so that the peak count rate is located at $t=0$ and the FWHM point of the decay portion is located at $t=0.2$. To obtain the value of r_{cv} in a pulse, we evaluate the first order derivatives, $C'(\tau)$, of a pulse, and then identify the inflexion from concavity to convexity. Applied this method, we receive a list of the value of r_{cv} for our sample pulses, which is shown in Table 1. The distribution of r_{cv} is presented in Fig. 2.

According to Fig. 3, we divide our sample into 3 classes by the range of r_{cv} , which are named as class 1 ($r_{cv} \leq 0.5$), class 2 ($0.5 < r_{cv} \leq 2$) and class 3 ($r_{cv} > 2$). Their percentages to the total number are 5.8, 58.1 and 36.1, respectively. The observed distribution of r_{cv} , whose explanation is not clear, may constrain the mechanism of the birth of local pulses in both models.

Light curve and their slopes of three events, # 07374 ($r_{cv} = 0.42$), # 01883 ($r_{cv} = 1.69$) and # 01733 ($r_{cv} = 5.01$), are drawn in Fig. 4. One find that the characters of the slopes are in agreement with what we obtain in last section. This suggests that, at least for our sample sources, the curvature effect (or the Doppler effect of an expanding spherical surface) for a uniform jet or a spherical fireball is indeed at work.

Table 1. A list of the value of r_{cv} for our sample pulses

trigger number	r_{cv}	trigger number	r_{cv}	trigger number	r_{cv}
493	0.70	2665	0.80	5474	1.15
563	0.91	2700	3.53	5478	0.50
829	0.96	2749	11.29	5495	0.93
907	0.69	2880	7.85	5517	1.70
914	2.05	2919	1.48	5523	7.47
973	0.99	3040	1.31	5601	1.02
973	0.80	3143	6.19	5601	1.52
999	4.17	3155	0.76	6225	0.31
1157	7.75	3256	1.63	6335	2.84
1406	0.69	3237	1.44	6397	1.02
1467	2.71	3257	1.23	6504	0.70
1700	1.11	3415	0.66	6621	2.00
1733	5.01	3648	3.58	6672	1.26
1883	1.69	3668	2.87	6672	0.82
1956	1.56	3765	1.92	6930	1.70
1989	0.11	3866	4.20	7293	1.46
2083	4.68	3870	1.29	7295	1.51
2102	2.41	3875	0.63	7374	0.42
2138	1.99	3886	4.50	7403	0.65
2267	4.52	3892	0.85	7548	1.18
2306	4.90	3954	7.85	7548	0.70
2387	0.70	4157	1.36	7588	0.90
2393	7.28	4350	0.90	7638	3.80
2393	2.99	4350	2.75	7648	1.45
2431	6.0	4350	2.52	7701	4.72
2484	1.12	4368	1.02	7711	0.38
2519	4.07	4368	0.74	7744	10.74
2530	0.37	4710	0.89	8111	2.40
2662	1.19	5415	1.39		

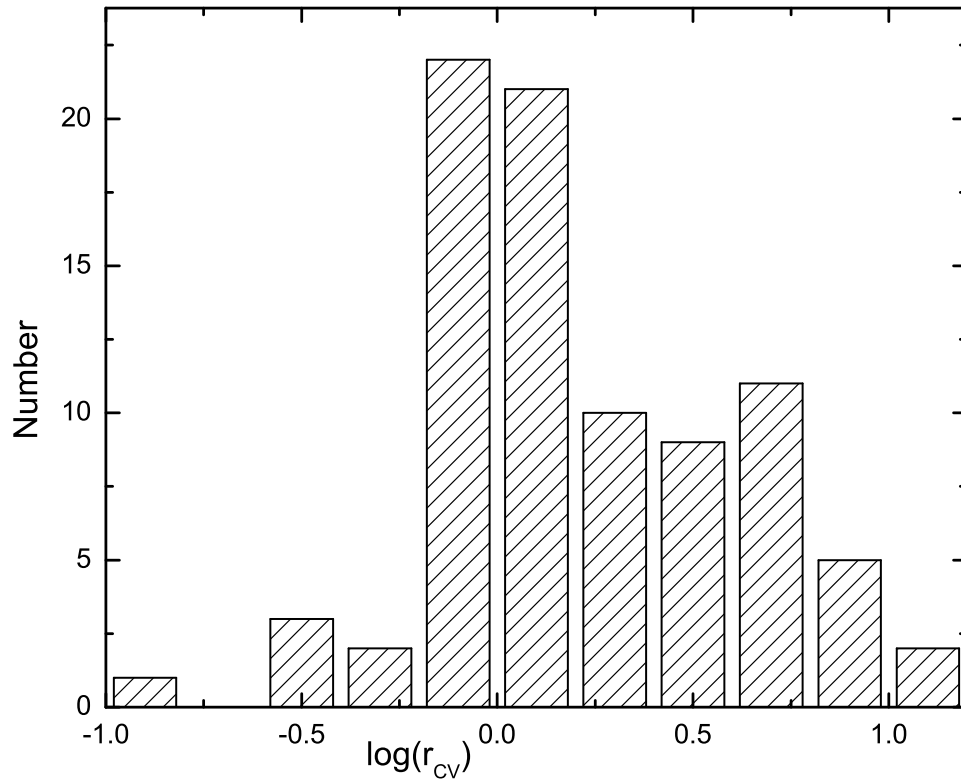


Figure 1. Distribution of r_{cv} of all pulses in our sample

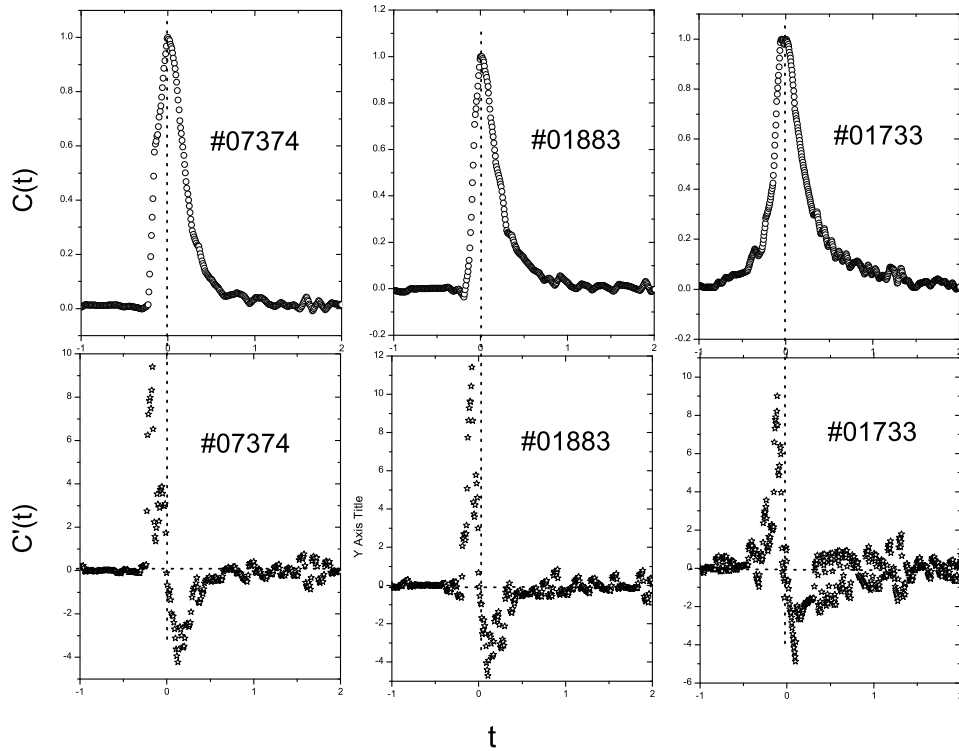


Figure 2. Plot of the normalized and re-scaled pulses (first row) and their slopes (second row) for several sample source.

4 DISCUSSION AND CONCLUSIONS

All analyses in this paper are based on formula (1), which is suitable for describing light curves of spherical fireballs or uniform jets. Numerical calculations show that the characters of light curves, the “concave-to-convex” one in the rising phase and the “convex-to-concave” one in the decay portion, are not affected by the Lorentz factor Γ and the half-opening angle θ_j .

Let us study the impact of rest frame radiation forms on a light curve profile. As a general radiation form observed, the Band function, for which, some sets of typical values of the indexes would represent certain mechanisms (see Band et al. 1993), will be employed. Here we take three sets of values of the indexes: $\alpha_0=-1$ and $\beta_0=-2.25$, $\alpha_0=-1$ and $\beta_0=-4.5$, $\alpha_0=-0.5$ and $\beta_0=-2.25$. The light curves, slopes, r_r and r_d , are plotted in Fig.5.

As shown in the figure, different rest frame radiation forms lead to different values of r_r and r_d , but the value of r_{cv} and the profile character mentioned above are not affected.

Zhang et al. (2002) found that a structured jet has the same temporal evolutions as the uniform jet has as long as the relativistic beaming angle $1/\Gamma$ is much smaller than the viewing angle θ_v , in this situation, the fireball is observed as if it were isotropic. We thus

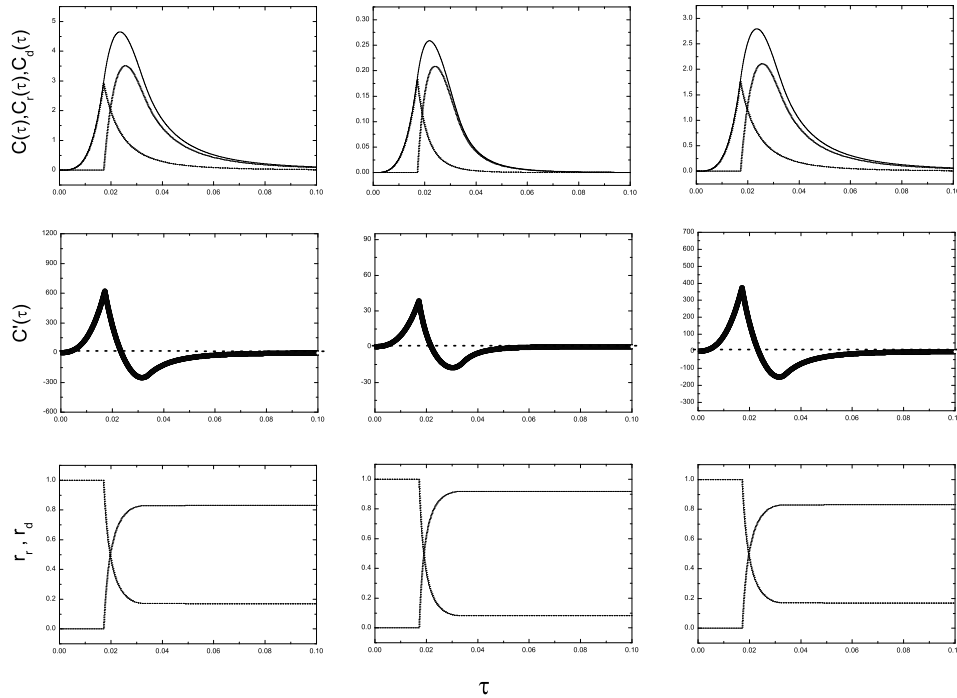


Figure 3. Plot of $C(\tau)$, $C_r(\tau)$, $C_d(\tau) - \tau$, $C'(\tau) - \tau$, r_r , $r_d - \tau$ for the light curve of the power law local pulse determined by (2), where a Band function rest frame form is adopted. And we take $\Gamma=10$, $\mu = 2$, $\Delta\tau_{\theta,FWHM}=2$, $\tau_{\theta,min}=0$, $\tau_{\theta,max}=2$. $\tau_{\theta,0}=\tau_{\theta,max} * 0.5$. $\alpha_0=-1$ and $\beta_0=-2.25$ (for first column), $\alpha_0=-1$ and $\beta_0=-4.5$ (for second column), $\alpha_0=-0.5$ and $\beta_0=-2.25$ (for last column). The symbols are the same as those adopted in Fig.1.

suspect that the characteristics of light curves in the structure jet may probably be similar to those obtained above, which deserves a detailed analysis.

One may ask whether or not the characteristics of the profile of light curves come from the intrinsic behavior. Our analysis shows that it is not the case. Taking $\mu = 1$ in equation (2), which become a linear rise and a linear local pulse, the characters are the same as in the case of $\mu = 2$. The fact shows that the characteristics indeed result from the curvature effect, instead of being an intrinsic one.

We come to the conclusion that, the light curve characteristics, a “concave-to-convex” curve in the rising portion and a revers curve in the decay portion, which is independent of the shapes of local pulses, exist in the observed light curve of some GRBs (We find 86 source in our sample). We believe that reverse characters in both portions (Say, a “convex-to-concave” curve in the rising portion and a “concave-to-convex” curve in the decay part) would never be detected if the radiated surface is a spherical one, regardless of a spherical fireball or a uniform jet. The characters could serve as an indicator of the curvature effect or the Doppler effect.

This work was supported by the Special Funds for Major State Basic Research Projects (“973”) and National Natural Science Foundation of China (No. 10273019).

REFERENCES

- Band, D., Matteson, J., Ford, L., Schaefer, B., Palmer, D., Teegarden, B., Cline, T., Briggs, M., et al. 1993, ApJ, 413, 281
- Bloom, J., Frail, D. A., & Kulkarni, S. R. 2003, ApJ, 588, 945
- Borgonovo, L., & Ryde, F. 2001, APJ, 548, 770
- Fenimore, E., Epstein, R., & Ho, C. 1993, A&AS, 97, 59
- Fenimore, E. E., Madras, C. D., and Nayakshin, S. 1996, ApJ, 473, 998
- Fishman, Gerald J., Meegan, Charles A., Wilson, Robert B., Brock, Martin N., Horack, John M., Kouveliotou, Chryssa, Howard, Sethanne, Paciasas, William S. et al. 1994, ApJS, 92, 229
- Fishman, G., Meegan, C. 1995, ARA&A, 33, 415
- Ford, L. A., Band, D. L., Matteson, J. L., et al. 1995, ApJ, 439, 307
- Frail, D., et al. 2001, ApJ, 562, L55
- Friedman, A. S., Bloom, J.S., 2004, astro-ph/0408413
- Fruchter, A. S., et al. 1999, APJ, 519, L13
- Harrison, F. A., et al. 1999, ApJ, 523, L121
- Kocevski, D., Ryde, F., and Liang, E. 2003, ApJ, 596, 389
- Lamb, D. Q., Donaghy, T. Q., & Graziani, C., 2005, ApJ, 620, 355
- Lee, A., Bloom, E. D., & Petrosian, V. 2000a, ApJS, 131, 1
- Lee, A., Bloom, E. D., & Petrosian, V. 2000b, ApJS, 131, 21
- Norris, J. P., Nemiroff, R. J., and Bonnell, J. T. et al. 1996, ApJ, 459, 393
- Panaiteescu, A., Kumar, P. 2001, APJ, 560, L49
- Piran, T. 1995, in AIP Conf. Proc. 307, Gamma-Ray Bursts: Second Huntsville Workshop, ed. G. J. Fishman, J. J. Brainerd, & K. Hurley (New York: AIP), 495
- Piran, T. 1999, Phys. Rep., 314, 575
- Preece, R. D., Pendleton, G. N., Briggs, M. S., et al. 1998, ApJ, 496, 849
- Preece, R. D., Briggs, M. S., Mallozzi, R. S., et al. 2000, ApJS, 126, 19
- Qin, Y.-P. 2002, A&A, 396, 705
- Qin, Y.-P. 2003, A&A, 407, 393
- Qin, Y. P., Zhang Z. B., Zhang F. W. and Cui X. H. 2004, APJ, 617, 439
- Ramirez-Ruiz, E., & Lloyd-Ronning, N. 2002, NewA, 7, 197
- Rossi, E., Lazzati, D., & Rees, M. J. 2002, MNRAS, 332, 945
- Ryde, F., and Petrosian, V. 2002, ApJ, 578, 290
- Ryde, F., and Svensson, R. 2000, ApJ, 529, L13
- Ryde, F., and Svensson, R. 2002, ApJ, 566, 210
- Sari, Re'em, Piran, Tsvi, Halpern, J. P. 1999, ApJ, 519L, 17S
- Schaefer, B. E., Teegaeden, B. J., Fantasia, S. F., et al. 1994, ApJS, 92, 285
- Stanek, K. Z., Garnavich, P. M., Kaluzny, J., Pych, W., Thompson, I. 1999, ApJ, 522, L39
- Waxman, E., Kulkarni, S. R., Frail, D. A. 1998, APJ, 497, 288
- Zhang, B., & Meszaros, P. 2002, ApJ, 571, 876
- Zhang, B., Dai, X., Lloyd-Ronning, N. M., & Meszaros, P. 2004a, ApJ, 601, L119
- Zhang, W., Woosley, S. E., & Heger, A. 2004b, ApJ, 608, 365